

**“CLASSICAL” VORTEX NUCLEATION IN SUPERFLOW
THROUGH SMALL ORIFICES**

Michael Stone

Department of Physics

University of Illinois at Urbana Champaign

1110 W. Green St.

Urbana, IL 61801

USA

&

Ajit M. Srivastava

Institute of Physics

Sachivalaya Marg

Bhubaneswar 751005

INDIA

Abstract

We report on numerical solutions of the Gross-Pitaevskii equation for two-dimensional flow of a superfluid condensate through a small orifice. Above a critical velocity of about 30% of the speed of sound, cavitation occurs in the throat of the orifice. The cavitating bubbles form the cores of singly quantized vortices which detach from the boundary and are convected downstream.

1. Introduction

Boundary layer separation is a familiar phenomenon in classical fluid dynamics [1]. It is invariably associated with the appearance of vorticity in the bulk of the fluid. The main flow and the relatively stagnant fluid in the lee of the bounding body may be in irrotational motion but they are separated by the detached boundary layer, a sheet of fluid containing vorticity generated by viscous forces while it was in contact with the body. For example, when a classical fluid is forced through a small opening the flow separates close to the narrowest point of the orifice and forms a jet penetrating into the ambient fluid. This jet is bounded by a tube of vorticity which confines the flow much as a solenoid confines the magnetic field it produces. When the opening has a sharp salient edge the boundary layer separation takes place at arbitrarily low flow velocities. If the edge is rounded there will be some critical velocity below which the flow remains attached and potential.

Similar regimes occur when a superfluid is forced through a small opening. At low velocities the superflow is potential and dissipationless. Liquid can pass through the orifice without the need for a pressure difference between the two sides. Above a critical flow rate a pressure head is needed to maintain the flow. At sufficiently high flow rate even a superfluid behaves as a classical liquid, and in this regime we can be confident that a collimated jet has formed. Because vorticity is quantized in a superfluid, the flow separation requires the shedding of discrete vortices from the boundary. These vortices will approximate the classical vortex sheet bounding the the jet, just as the individual windings approximate an ideal solenoid.

In recent years resonators containing micron sized orifices have been constructed in which one can monitor the dissipation produced by the shedding of a single vortex [2,3]. At very low temperatures the critical velocities in the orifice become independent of temperature, and this temperature independence is cited as evidence that the vortices are being created by quantum mechanical tunneling [4,5]. This inference is probably correct, but it is worth appreciating that thermal or quantum nucleation are not the only alternatives for creating a vortex. Vortices may also be shed from a boundary via cavitation. An accurate estimate of the critical velocity for this “classical” vortex creation mechanism is needed before one can state with confidence that one is seeing macroscopic quantum tunneling events.

This present paper provides a rough estimate of this critical velocity. It reports numerical solutions of the time-dependent Gross-Pitaevskii (G-P) equation [6,7] for flow through (two dimensional) orifices. These solutions demonstrate that when the velocity near the classical flow separation point exceeds about 30% of the speed of sound, low pressure in the throat of the orifice causes cavitation. Pairs of bubbles are

pulled off the boundary, the pair forming the core of what in three dimensions would be a singly-quantized smoke-ring-like vortex.

It is surprising that this classical cavitation effect was not discovered long ago. It is not described in any of the standard references on the G-P equation but, while we were performing the calculations reported here, our attention was drawn to the recent work of Frisch, Pomeau and Rica who observed similar vortex shedding from the boundary of cylinders immersed in a uniform flow [8,9]. These authors interpret the vortex shedding as a substitute for shock-wave solutions (which do not occur in the G-P equation) rather than, as seems more natural to us, an emulation of boundary layer separation. Also they do not exhibit detailed pictures of the formation of the vortices. Consequently, in addition to readvertizing the phenomenon and estimating the critical velocity, we include some detailed plots of how the order parameter phase evolves as the vortices form. In the second section we will review the well-known interpretation of the real and imaginary parts of the Gross-Pitaevskii equation as the equations of fluid mechanics. We also include a discussion of the Josephson phase winding between the core of a jet and the ambient fluid. In the third section we will report on the numerical methods and boundary conditions used to induce the flows. In the fourth section we describe the results.

2) The Gross-Pitaevskii equation

The Gross-Pitaevskii (G-P) non-linear Schrödinger equation [6,7] provides a simple model for the dynamics of the condensate in ${}^4\text{He}$. Although the local version of this equation does not describe the roton part of the quasiparticle spectrum [9], it does model the most essential ingredients: long-range phase coherence coupled with mass and momentum conservation.

To establish our notation, and to develop some physical insight, we begin by reviewing the close relationship between the G-P equation and classical fluid dynamics. Because it is important to distinguish between quantum and classical effects we will include explicit factors of \hbar . For generality we will also include a coupling to a gauge field, although the application in this paper is primarily to neutral superfluid ${}^4\text{He}$.

The Gross-Pitaevskii equation is the non-linear Schrödinger equation of the form

$$i\hbar(\partial_t - ieA_0/\hbar)\Psi = -\frac{\hbar^2}{2m} \sum_{a=1}^3 (\partial_a - ieA_a/\hbar)^2 \Psi + \lambda(|\Psi|^2 - \rho_0)\Psi. \quad (1.1)$$

The sign of λ will be understood to be positive, so the last term in (1.1) represents a repulsive force between the ${}^4\text{He}$ atoms. (This is the opposite sign from that usually taken when studying the one-dimensional

non-linear Schrödinger equation as an example of an integrable soliton system.) The mass m should be taken to be that of a helium atom (6.647×10^{-27} kg). The values of λ , and the number density ρ_0 are usually chosen to fit the measured density ($m\rho_0 = 145 \text{ kg m}^{-3}$), and speed of sound ($c = \sqrt{\lambda\rho_0/m} = 230 \text{ ms}^{-1}$) in the fluid.

By using the Madelung transformation [10], (1.1) can be recast as the equation of motion of a charged compressible fluid having equilibrium particle-number density ρ_0 . We set $\Psi = \sqrt{\rho}e^{i\theta}$ and define a velocity field \mathbf{v} in such a way that the number-current,

$$\mathbf{j} = \frac{\hbar}{2mi} (\Psi^*(\nabla - ie\mathbf{A}/\hbar)\Psi - ((\nabla + ie\mathbf{A}/\hbar)\Psi^*)\Psi), \quad (1.2)$$

may be written as $\mathbf{j} = \rho\mathbf{v}$. This requires

$$\mathbf{v} = \frac{\hbar}{m}(\nabla\theta - e\mathbf{A}/\hbar). \quad (1.3)$$

In the absence of vortex singularities in Ψ , the vorticity, $\omega = \nabla \wedge \mathbf{v}$, is completely determined by the gauge field to be $\omega = -\frac{e}{m}\nabla \wedge \mathbf{A} = -\frac{e\mathbf{B}}{m}$, *i.e.*

$$m\omega + e\mathbf{B} = 0. \quad (1.4)$$

For neutral superfluids (1.4) implies irrotational motion and hence, at low velocities, where the effects of compressibility can be ignored, leads to D'Alembert's paradox (the absence of drag forces). For charged superfluids equation (1.4) is responsible for the Meissner effect: A penetrating uniform \mathbf{B} field would require uniform vorticity, *i.e.* rigid rotation. A rigidly rotating body possesses a kinetic energy which grows faster than the volume of the system and so is impossible in the thermodynamic limit. Alternatively, taking the curl of the Maxwell equation $\nabla \wedge \mathbf{B} = e\mathbf{j}$ and using $\mathbf{j} = \rho\mathbf{v}_s$ together with (1.4), implies that

$$\nabla^2\mathbf{B} - \frac{e^2\rho}{m}\mathbf{B} = 0, \quad (1.5)$$

which leads to flux screening. Note that \hbar does not appear in (1.4) or in the screening length $(e^2\rho/m)^{-1/2}$.

With the definition (1.3), the imaginary and real parts of (1.1) become, respectively, the continuity equation

$$\partial_t\rho + \nabla \cdot \rho\mathbf{v} = 0, \quad (1.6)$$

and the Euler equation governing the flow of a barotropic fluid

$$m(\partial_t\mathbf{v} + \mathbf{v} \cdot \nabla\mathbf{v}) = e(\mathbf{E} + \mathbf{v} \wedge \mathbf{B}) - \nabla\mu. \quad (1.7)$$

The word *barotropic* refers to the simplifying property that the pressure term $\frac{1}{\rho}\nabla P$, which occurs on the right hand side of the conventional Euler equation, is here combined into the gradient of a potential

$$\mu \equiv \lambda(\rho - \rho_0) - \frac{\hbar^2}{2m} \frac{\nabla^2 \rho}{\rho}. \quad (1.8)$$

The potential μ contains the expected compressibility pressure, depending on the deviation from the equilibrium density, together with a correction depending on gradients of ρ . This correction, the *quantum pressure*, is the only place that \hbar appears in the flow equations. It sets the length scale $\xi = \hbar/\sqrt{2m\lambda\rho_0}$ over which the superfluid density heals after being forced to zero by a boundary or a vortex singularity. With the parameters chosen as suggested above we find $\xi = .487 \text{ \AA}$. (\hbar also manifests itself, of course, in the quantum of circulation, $\kappa = 2\pi\hbar/m$.)

The Euler equation (1.7) is derived by first taking the gradient of (1.1) and interpreting the result as the Bernoulli equation,

$$m(\partial_t \mathbf{v} - \mathbf{v} \wedge \boldsymbol{\omega}) = e(\mathbf{E} + \mathbf{v} \wedge \mathbf{B}) - \nabla \left(\frac{1}{2} m \mathbf{v}^2 + \mu \right), \quad (1.9)$$

which is equivalent to (1.7).

In (1.9) a cancellation of the $m\mathbf{v} \wedge \boldsymbol{\omega}$ term against the $e\mathbf{v} \wedge \mathbf{B}$ term is evident upon use of (1.4). It is after this cancellation, and so without reference to either \mathbf{B} or $\boldsymbol{\omega}$, that the hydrodynamic picture of superconductivity is conventionally displayed. It seems preferable to keep both $\boldsymbol{\omega}$ and B in (1.9) and rewrite it as (1.7). By doing this one can see that the only difference between superfluid dynamics and classical fluid dynamics lies in the constraint (1.4).

In the next section we solve (1.1) numerically for the case of a neutral superfluid forced to flow through an orifice. Let us first consider a crude model of the extreme case where the downstream flow forms a tubular jet penetrating into superfluid at rest.

We suppose that there is a pressure head, and correspondingly a difference $\mu_1 - \mu_0$ in the potential, between the asymptotic parts of the reservoirs communicating via the orifice. This means that the phase of the order parameter of the fluid at rest in the upstream reservoir, θ_1 , must be falling behind the phase of the order parameter in of the fluid at rest in the lower pressure container, θ_0 , at a rate given by

$$-\hbar \frac{d}{dt}(\theta_1 - \theta_0) = \mu_1 - \mu_0. \quad (1.10)$$

If the flow is steady, (1.9) implies that $\dot{\theta}$ is position independent. Consequently, as we follow a streamline through the orifice into the core of the jet, we must have the classical Bernoulli relation

$$\frac{1}{2} m v^2 + \mu = \text{const.} \quad (1.11)$$

Now the pressure in the jet and that of the adjacent ambient fluid must be the same, or the fluid would move sideways. This requires the value of μ in the jet to equal μ_0 . Thus the velocity of the fluid in the jet is given by

$$\frac{1}{2}mv^2 = \mu_1 - \mu_0, \quad (1.12)$$

a familiar classical result. We find then that

$$-\hbar \frac{d}{dt}(\theta_{jet} - \theta_{ambient}) = \frac{1}{2}mv^2. \quad (1.13)$$

This accumulating phase slip must be accounted for by the passage of vortices in the shear flow bounding the jet [11].

To verify this we note that the shear flow has vorticity v per unit length. Since θ winds through 2π as we encircle a vortex, the quantum of circulation is $2\pi\hbar/m$. There are therefore $mv/2\pi\hbar$ vortices per unit length in the jet boundary. Each of these vortices will be convected with the velocity field due to all the *other* vortices, and, by arguments familiar from the calculation of the force on the windings of a solenoid, this velocity is $v/2$. Thus smoke-ring-like vortices are shed at the orifice and convected downstream at a rate of $\frac{1}{2}mv^2/2\pi\hbar$ vortices per second. Each vortex allows a phase-slip of 2π , so the phase slip between points inside the jet and those outside accumulates at a rate $\frac{1}{2}mv^2/\hbar$, in comfortable conformity with (1.13).

This result is an example of Anderson's general relation, proved in Appendix B of [11], between the difference in the Bernoulli constant at two points and rate of passage of vortices across any curve connecting them.

3 Numerical Procedure and Results.

For the purpose of our numerical work we use the Gross-Pitaevskii equation in the following form.

$$i\partial_t\psi = -\nabla^2\psi + (|\psi|^2 - 1)\psi. \quad (3.1)$$

This corresponds to redefining the units for x and t , and the normalization of ψ . In these new units the speed of sound c is equal to $\sqrt{2}$. As we mentioned earlier, we confine our study to two space dimensions.

We implemented the time evolution using a stabilized leapfrog algorithm of second order accuracy. We used a 200×200 lattice with the lattice spacing in spatial directions chosen to be equal to 0.2 and the spacing in time direction equal to 0.004. Evolution was stable with these parameters and the total density

was conserved to within 1-2 percent during the evolution. The calculations were performed on SPARC 10 workstation at ITP Santa Barbara and on HP735 workstation at IOP Bhubaneswar.

We have studied three different cases corresponding to various geometries and sizes of the orifice. Figures 1a, 1b and 1c show the contour plots for the initial configurations of ψ corresponding to these three cases. The order-parameter phase, θ , is equal to zero everywhere for these initial configurations. A fixed boundary condition $\psi = 0$ is maintained at $x = 0$. At the other boundary in x direction ($x = 40$ in our simulations) free boundary conditions are used, while periodic boundary conditions are used in the y direction. The midpoint of the orifice is at $x = 20$. Figure 1a shows the case of orifice with sharp edges where $\psi = 0$ is kept fixed on a line along the y axis (at $x = 20$), leaving the opening for the orifice. Figure 1b shows the case when the edges of the orifice are semicircles, and Fig. 1c shows orifice, again with rounded edges, but with a wider opening. Dense regions of contours correspond to the healing length in which ψ grows from the value $\psi = 0$ to the value $|\psi| = 1$.

We begin by using a relaxation method to obtain initial solutions of the G-P equation with the boundary conditions described above. We evolve an initially chosen configuration using the diffusive equation

$$\partial_t \psi = \nabla^2 \psi - (|\psi|^2 - 1)\psi. \quad (3.2)$$

After about 2000 time steps $\psi(\mathbf{x})$ converges to a solution of the time independent G-P equation. These static solutions are the configurations shown in figures 1a, 1b and 1c. They become the initial condition for ψ for the time evolution using equation (3.1).

We tried several procedures for generating a superflow. Our first attempt utilised a piston moving along the positive x axis from $x = 0$. The piston was given a small uniform acceleration until it reached a suitable velocity. Shedding of vortex-antivortex pairs was observed using this method. Unfortunately, because of the finite size lattice, a constant piston velocity led to an increasing average velocity for the superflow through the orifice. This method, therefore, was not very suitable in determining the final asymptotic velocity of the superfluid through the orifice.

The second method consisted of the addition of a source term of the form $iw\psi/|\psi|^2$ to the G-P equation. Here, w is the strength of the source which is taken to be zero initially and increased slowly to a suitable maximum value during the course of the simulation. The source was taken to be non-zero along the line $x = 0.4$. This greater control allowed by this procedure provided a constant average superfluid velocity. The results reported in the following paragraphs make use of this method.

While we used equation (3.1) in most of the region we found it convenient to use the diffusive equation (3.2) in the large x region. This helped to damp out sound waves so that the vortex shedding could be studied in detail for large time durations. For the orifice with sharp edges, equation (3.1) was used for region between $x=0$ to $x=30$, while equation (3.2) was used between $x=30$ to $x=40$. For orifices with rounded edges, these regions were respectively $x=0$ to $x=35$ and $x=35$ to $x=40$. Since the dissipative equations were used for regions sufficiently far from the orifice, in the direction of the flow, it did not interfere with the process of vortex shedding.

Figures 2, 3 and 4 show the details of the process of vortex shedding for the three types of orifices. In these plots, solid lines are used to plot contours of ρ and dashed lines are used for θ contours. As described above, bubbles are pulled off the edges of the orifice. These form the cores of an vortex-antivortex pair which detaches from the edge and is swept along the flow. It is interesting to note that, for the orifice with rounded edges, vortex shedding does not occur at the point of smallest opening, but further downstream. This is not uncommon in boundary layer separation phenomena. It would be interesting to investigate what factors determine the point of vortex shedding for such cases.

Figures 5a, 5b, and 5c show the plots of the average velocity of the fluid flow through the different orifices as a function of time. We see that the flow increases uniformly, reaching, on the average, a critical velocity asymptotically. This critical velocity is roughly 0.4 (recall $c = 1.414$) for all three cases, irrespective of the shape of the edges of the orifice, or the size of the opening. We see that the fluid velocity first increases, and then there is a sudden decrease in the velocity. Looking at the contour plots at these times we see that the sharp decrease in the velocity coincides with the shedding of a vortex-antivortex pair. Actually, for rounded edges (figures 4b and 4c), the vortex shedding slightly precedes the drop in the fluid velocity. This is not unexpected as the vortex is produced downstream from the midpoint of the orifice, while the fluid velocity is calculated at the midpoint. It will take a while before the vortex shedding can affect the midpoint velocity. This further supports the idea that the drop in fluid velocity is caused by vortex shedding. Each successive large jump in the fluid velocity corresponds to a vortex-antivortex pair being shed.

An intuitive understanding of this sudden jump in the fluid velocity can be given in the following way. As the core of the vortex buldges out of the edge, it effectively narrows the orifice. This leads to an increase in the fluid velocity through the orifice which in turn further lowers the pressure. Eventually the vortex is shed and the backwards fluid motion around the vortex tends to reduce the net flow through the orifice. A significant part of the kinetic energy of the flow is transferred to the vortex.

4. Discussion

The vortex shedding process exhibited in this paper is probably not directly relevant for interpreting the experiments. The critical velocities reported in refs. [4,5] seem too low to cause cavitation. It is more likely that some form of quantum tunneling pre-empts the classical mechanism. It is, however, well worth obtaining a better understanding of the classical mechanism. The spontaneous shedding of vortices seen in our computation demonstrates that, at least for G-P fluids in two dimensions, the tunneling barrier to creating a vortex disappears above some critical velocity. This critical velocity needs to be estimated if the purely classical effect is to be distinguishable from the more interesting macroscopic quantum tunneling.

How does the vortex tunnel? Homogeneous quantum nucleation [12,13] is not possible when there is no normal fluid to select a preferred reference frame, but there are several competing channels that use the boundary to break galilean invariance. One possibility is to create a complete vortex ring surrounding the orifice. This, however, requires a large action. A more popular scenario is the quantum nucleation of a semicircular segment of vortex terminating on the boundary [14,15,16,17]. This segment is then swept into the flow where it grows by extracting energy from the bulk motion. Because this likely scenario breaks the axial symmetry, two-dimensional computations are not adequate for determining the classical critical velocity — if it exists. (Both the thin vortex models of [14,15] and the static G-P analysis in [16] suggest that a tunneling barrier persists even for large flow velocities.) It is therefore essential to perform a full three-dimensional time-dependent computation for an orifice with a suitable asperity on which the vortex can form.

Acknowledgements

Part of this work was carried out at the ITP Santa Barbara and we would like to thank the staff and members of the ITP for their hospitality. We were supported by the National Science Foundation under grant numbers PHY89-04035 (ITP) and by DMR91-22385 and its successor DMR94-24511 (University of Illinois). We would also like to thank Nigel Goldenfeld for alerting us to the existence of refs [8,9].

References

- [1] For example see: G. K. Batchelor *An Introduction to Fluid Mechanics*. (Cambridge University Press

167) Chapter 5.

- [2] W. Zimmermann Jr.; O. Avenel, E. Varoquaux, *Physica B* **165** (1990) 749; E. Varoquaux, O. Avenel, *Physica B* **197** (1994) 306.
- [3] A. Amar, Y. Sasaki, R. L. Lozes, J. C. Davis, R. E. Packard, *Phys. Rev. Lett.* **68** (1992) 2624.
- [4] J. C. Davis, J. Steinhauer, K. Schwab, Yu. M. Mukharsky, A. Amar, Y. Sasaki, R. E. Packard, *Phys. Rev Lett.* **69** (1992) 323.
- [5] G. G. Ihas, O. Avenel, R. Aarts, R. Salmelin, E. Varoquaux, *Phys. Rev. Lett.* **69** (1992) 327.
- [6] L. P. Pitaevskii, *Zh. Eksp. Teor. Fiz.* **40** (1961) 646, Translated in *Sov. Phys. JETP* **13** (1961) 451.
- [7] E. P. Gross, *Nuovo Cimento* **20** (1961) 454; *J. Math Phys.* **4** (1963) 195.
- [8] T. Frisch, Y. Pomeau, S. Rica, *Phys. Rev. Lett.* **69** (1992) 1644.
- [9] Y. Pomeau, S. Rica, *Phys. Rev. Lett.* **71** (1992) 247.
- [10] E. Madelung, *Z. Phys* **40** (1927) 322.
- [11] P. W. Anderson. *Rev. Mod. Phys.* **38** (1966) 298.
- [12] J. S. Langer, M. E. Fisher, *Phys. Rev. Lett.* **19** (1967) 560.
- [13] J. S. Langer J. D. Reppy, *Progress in Low Temperature Physics* **6** (1970) 1.
- [14] G. Volovik, *Pis'ma, Zh. Eksp. Teor Fiz* **15** (1972) 116 (*JETP Letters* **15** (1972) 81).
- [15] C. M. Muirhead, W. F. Vinen, R. J. Donnelly, *Phil Trans. Roy. Soc.* **A311** (1984) 433.
- [16] M. Bernard, S. Burkhart, O. Avenel, E. Varoquaux, *Physica B* **194-196** (1994) 499; *Phys. Rev. Lett.* **72** (1994) 380.
- [17] K. W. Schwarz, *Physica B* **197** (1994) 324; *Jour. Low Temp. Phys.* **93** (1993) 1019; *Phys. Rev. Lett.* **71** (1993) 259.

Figure Captions.

Fig 1. Initial configurations. The solid lines are contours of density.

Fig 2. Early stage of flow. The solid lines are contours of density. Dashed lines are contours of order-parameter phase. The heavy dashed lines are branch cuts where the order-parameter phase jumps through 2π .

Fig 3. Same as Fig 2., but at later time.

Fig 4. Same as Fig 3., but at later time.

Fig 5. Flow at midpoint of aperture. Each sharp dip in the velocity corresponds to a vortex-antivortex pair being shed.

Contour plot at t = 0.0

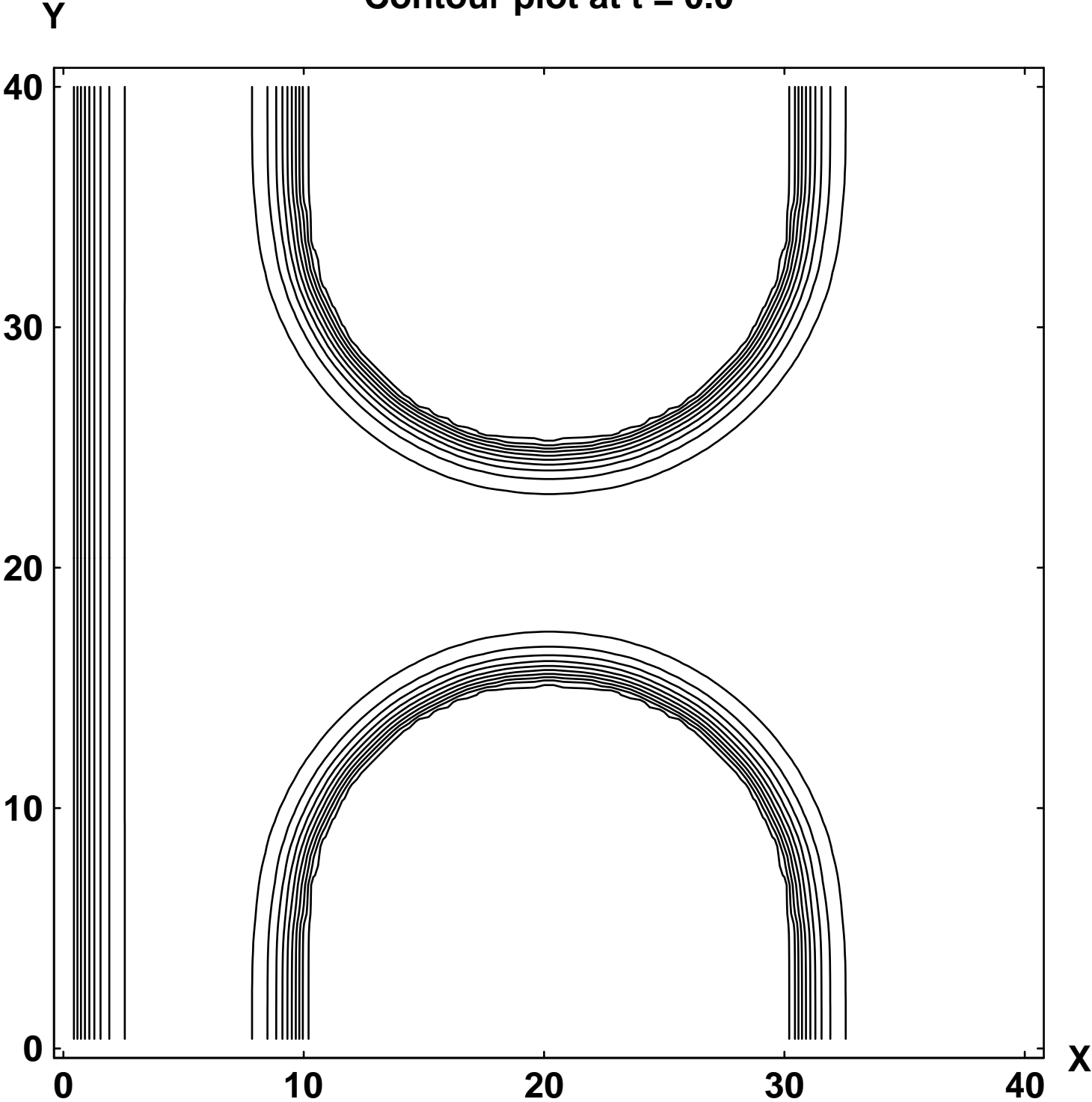


Fig. 1b

Contour plot at t = 79.0

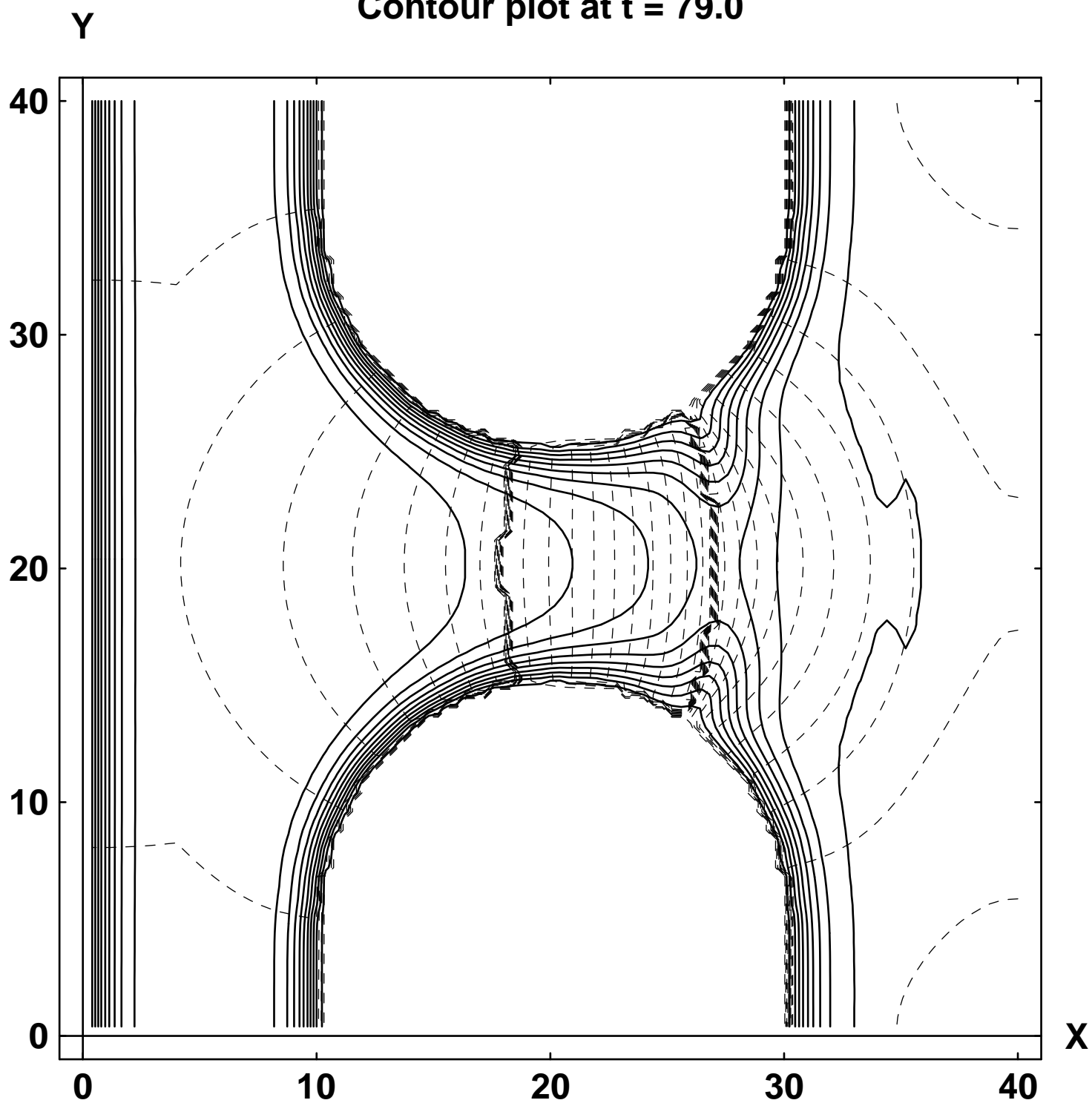


Fig. 2b

Contour plot at t = 68.0

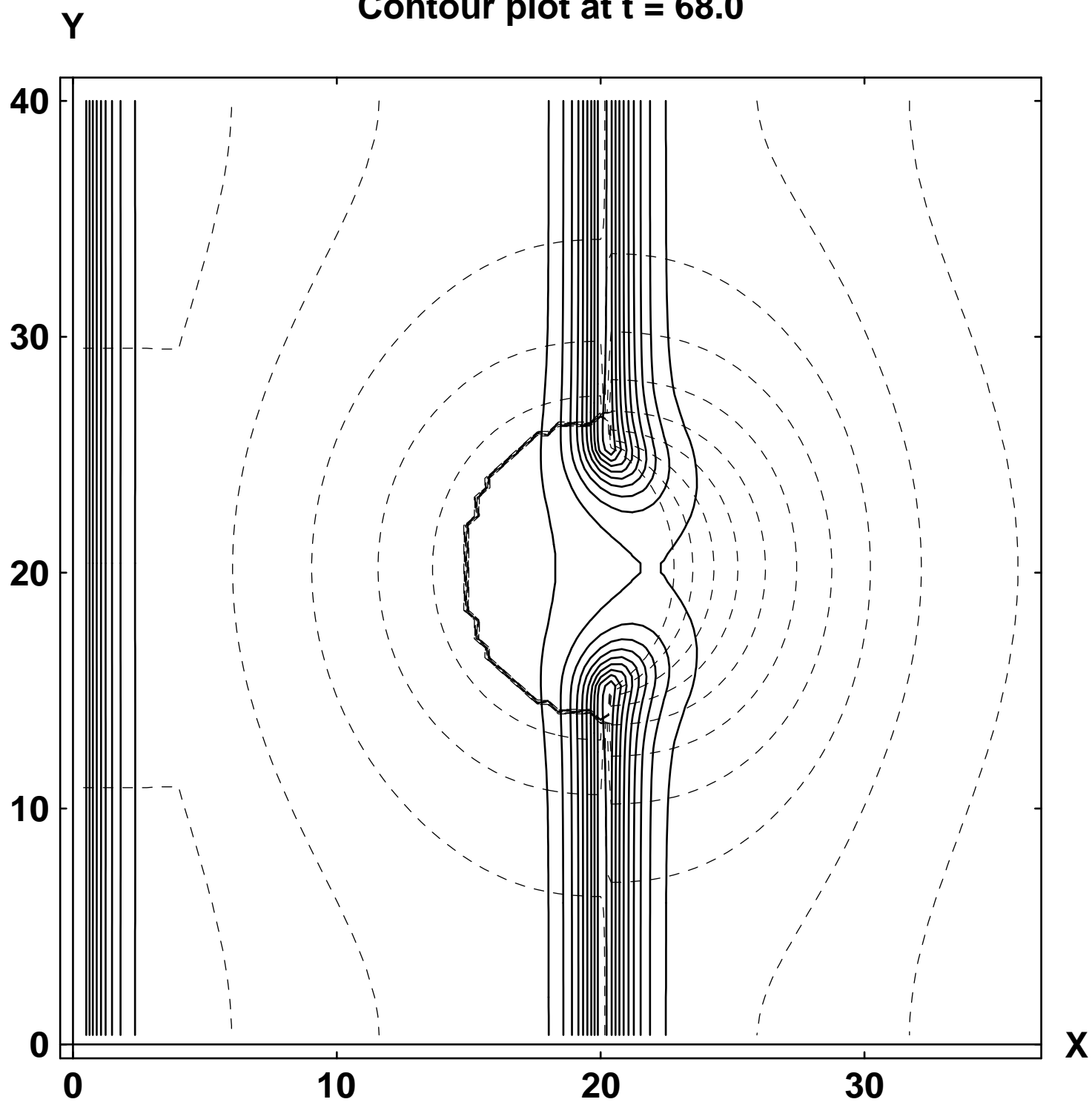


Fig. 2a

Contour plot at t = 82.0

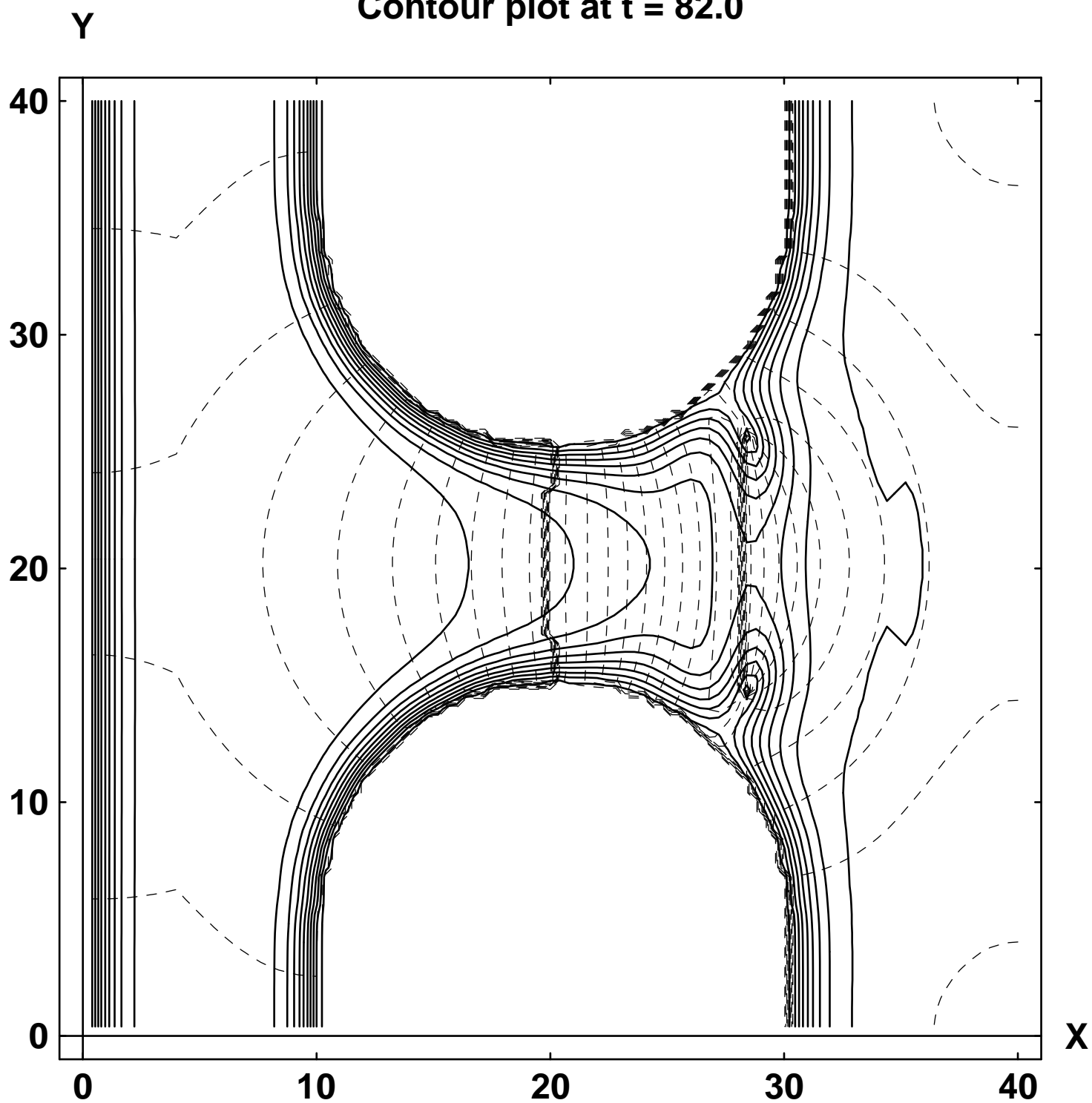


Fig. 3b

Contour plot at t = 72.0

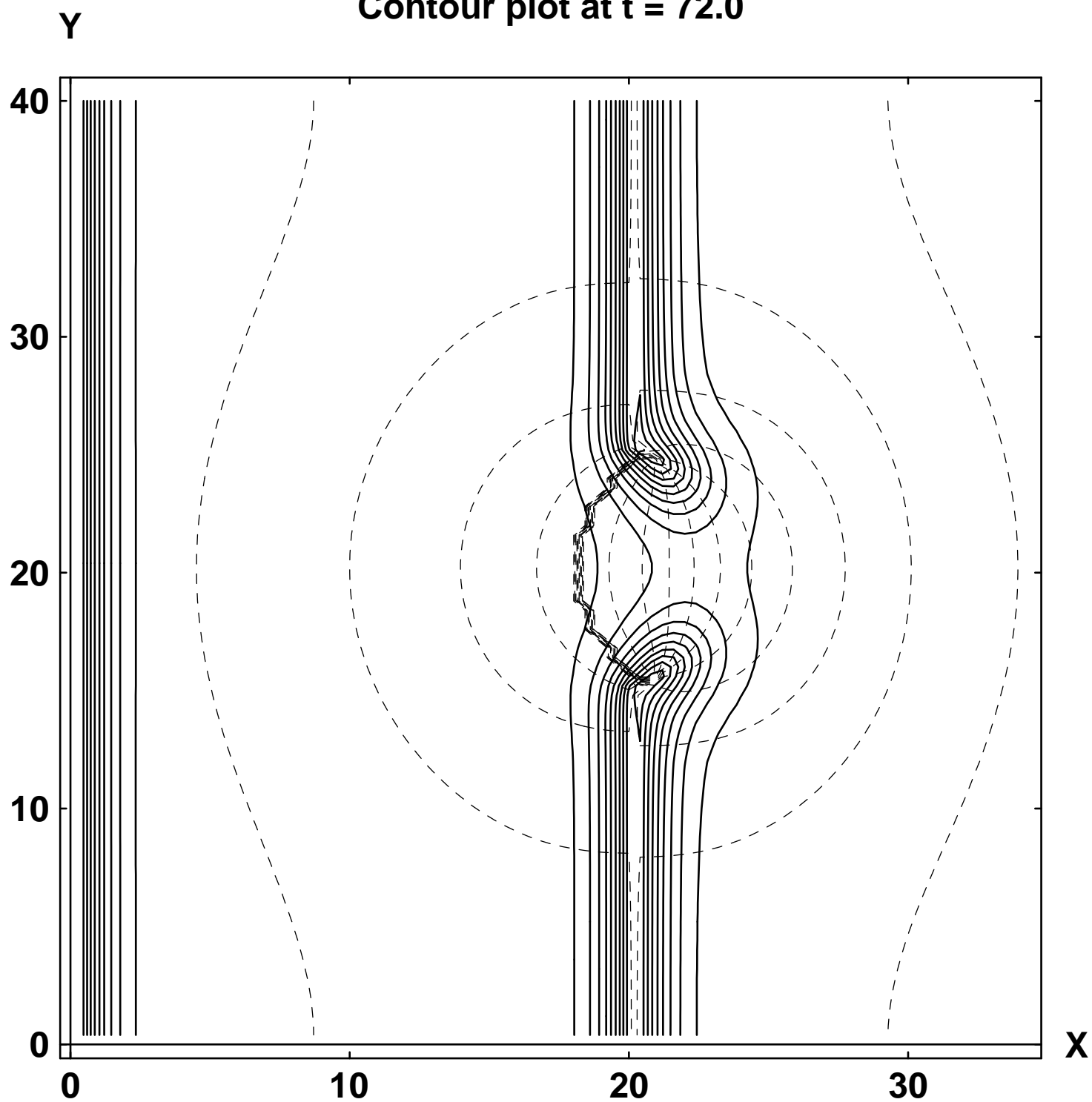


Fig. 3a

Contour plot at t = 84.0

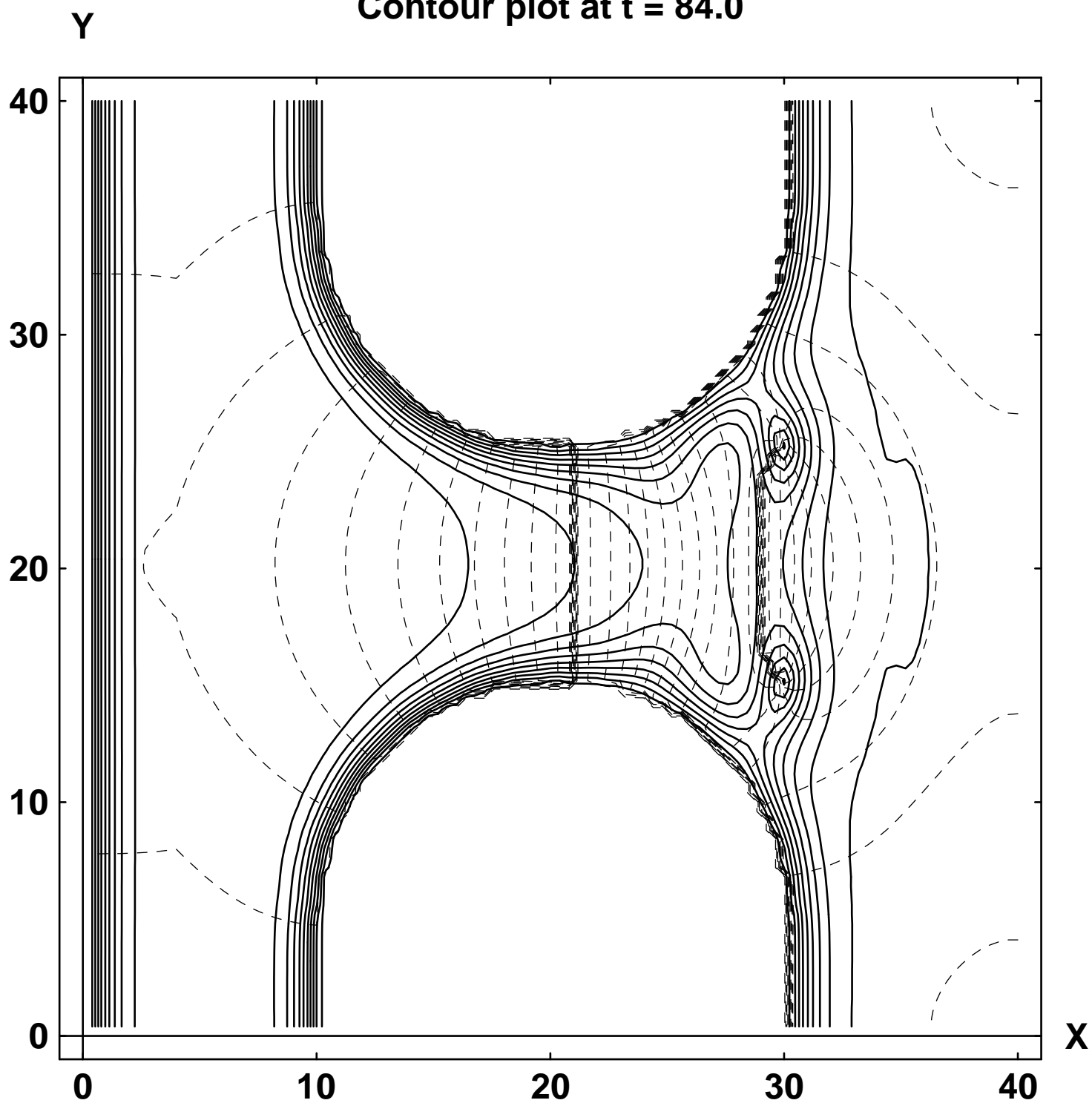
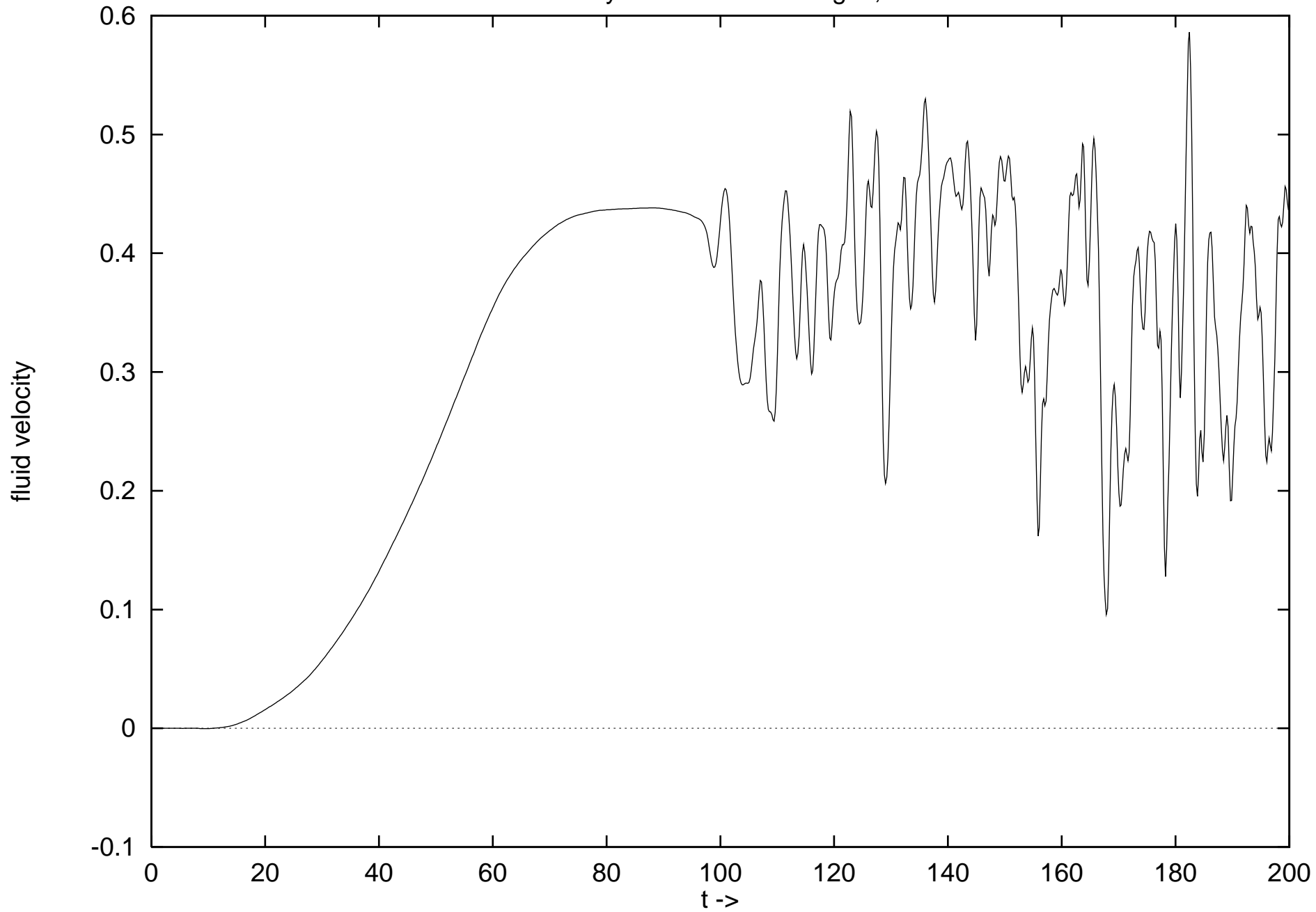


Fig. 4b

Plot of fluid velocity vs. time: round edges, narrow orifice



Contour plot at t = 0.0

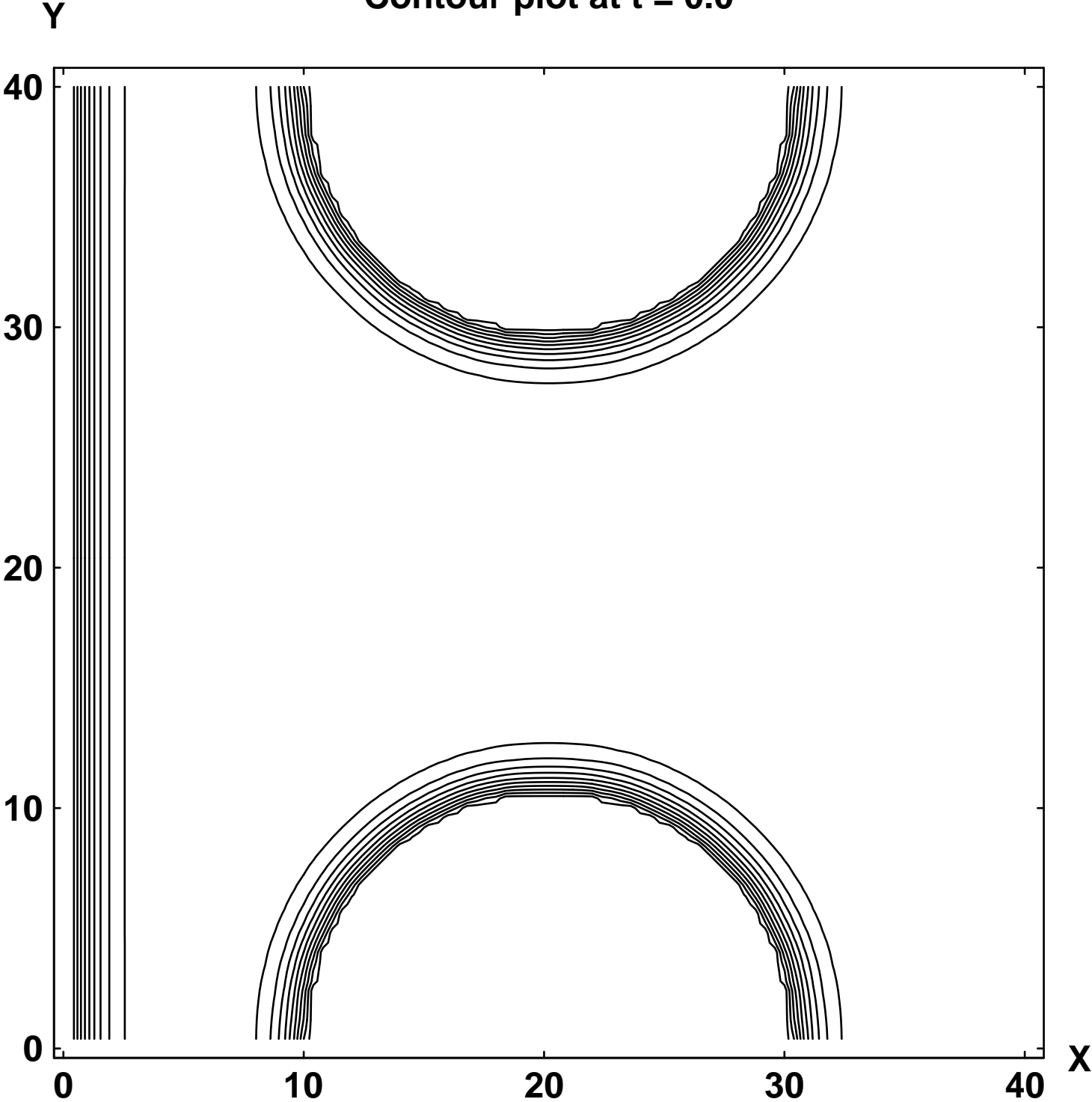


Fig. 1c

Contour plot at t = 58.0

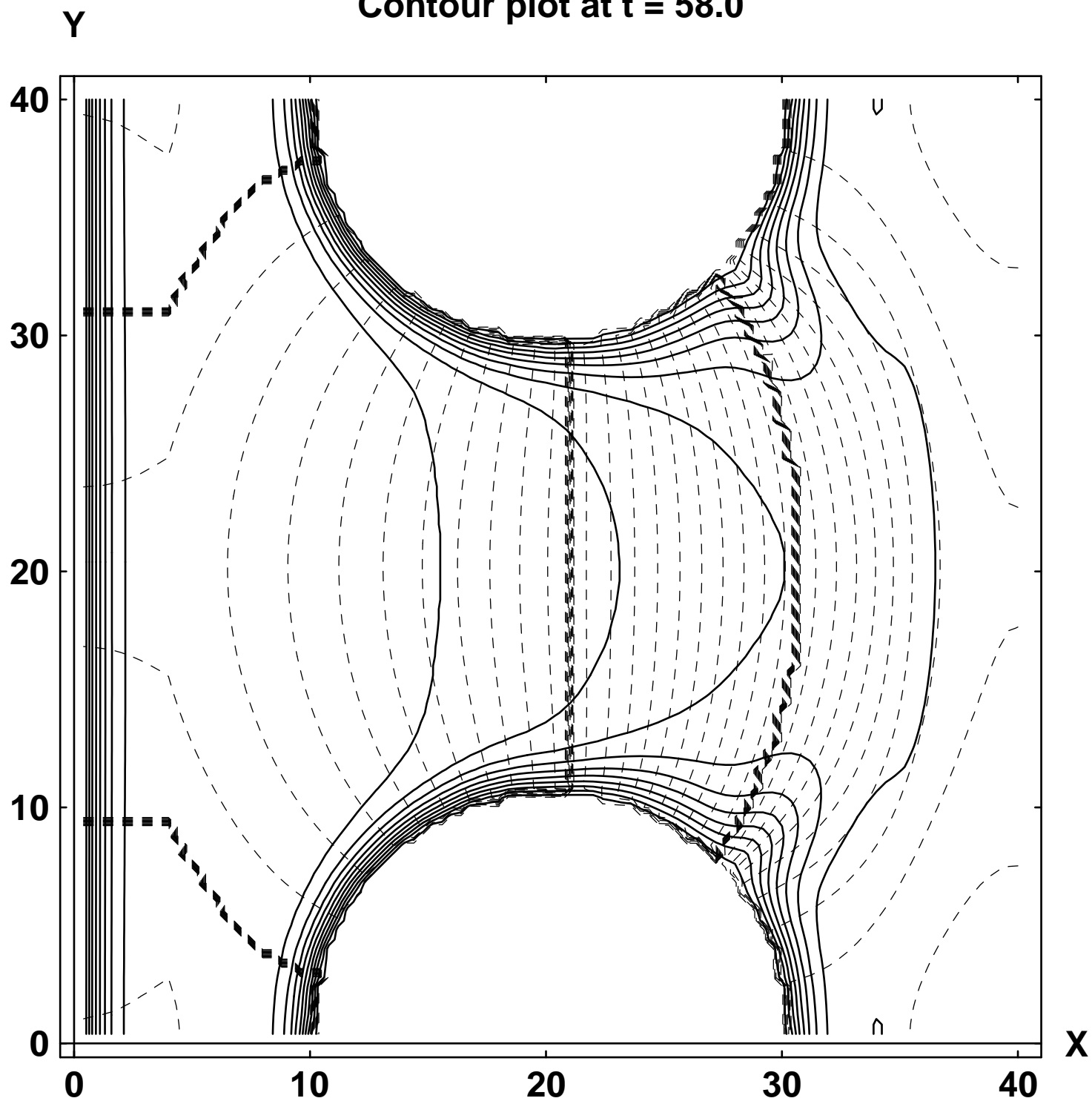


Fig. 2c

Contour plot at t = 62.0

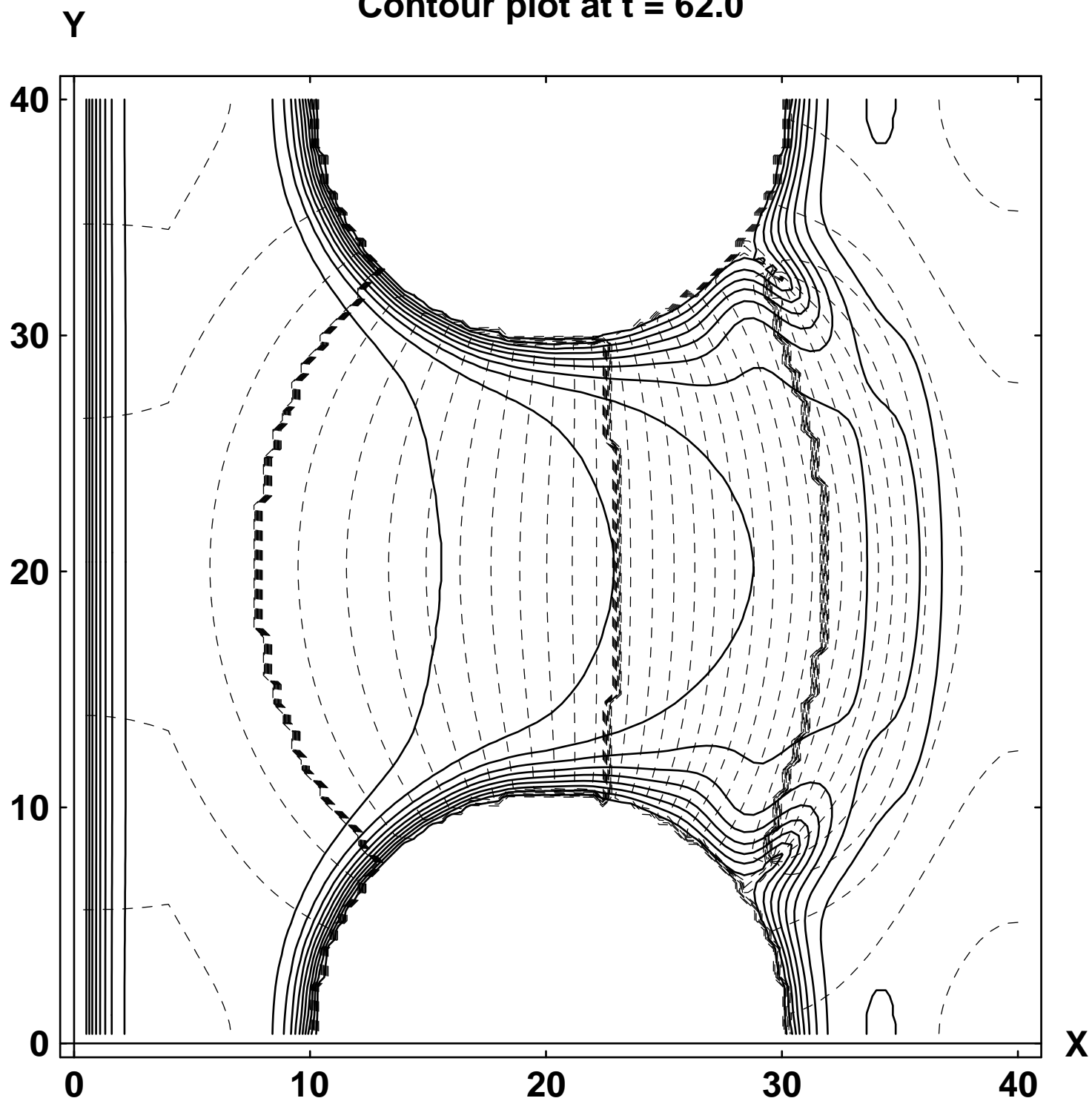


Fig. 3c

Contour plot at t = 64.0

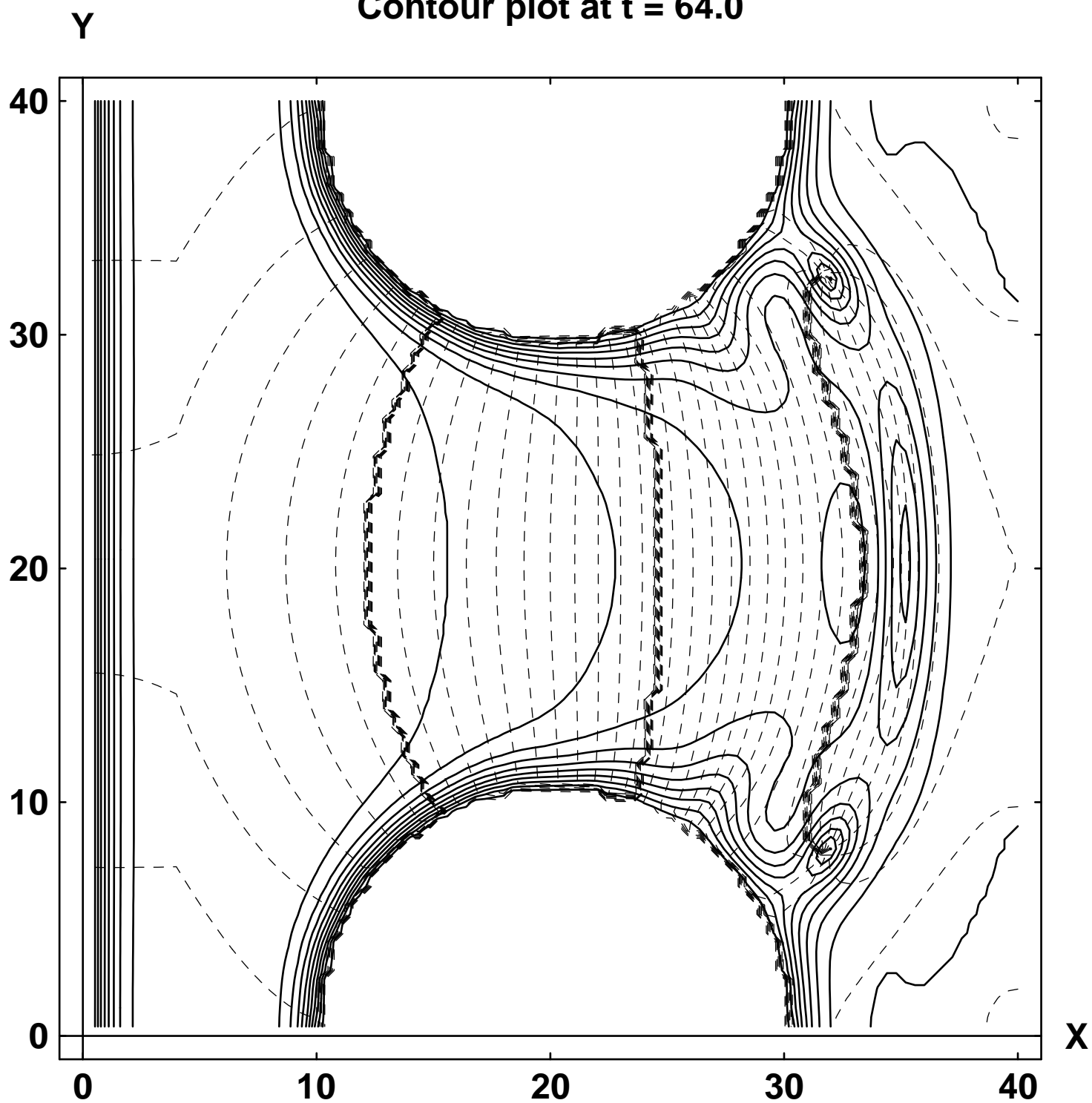
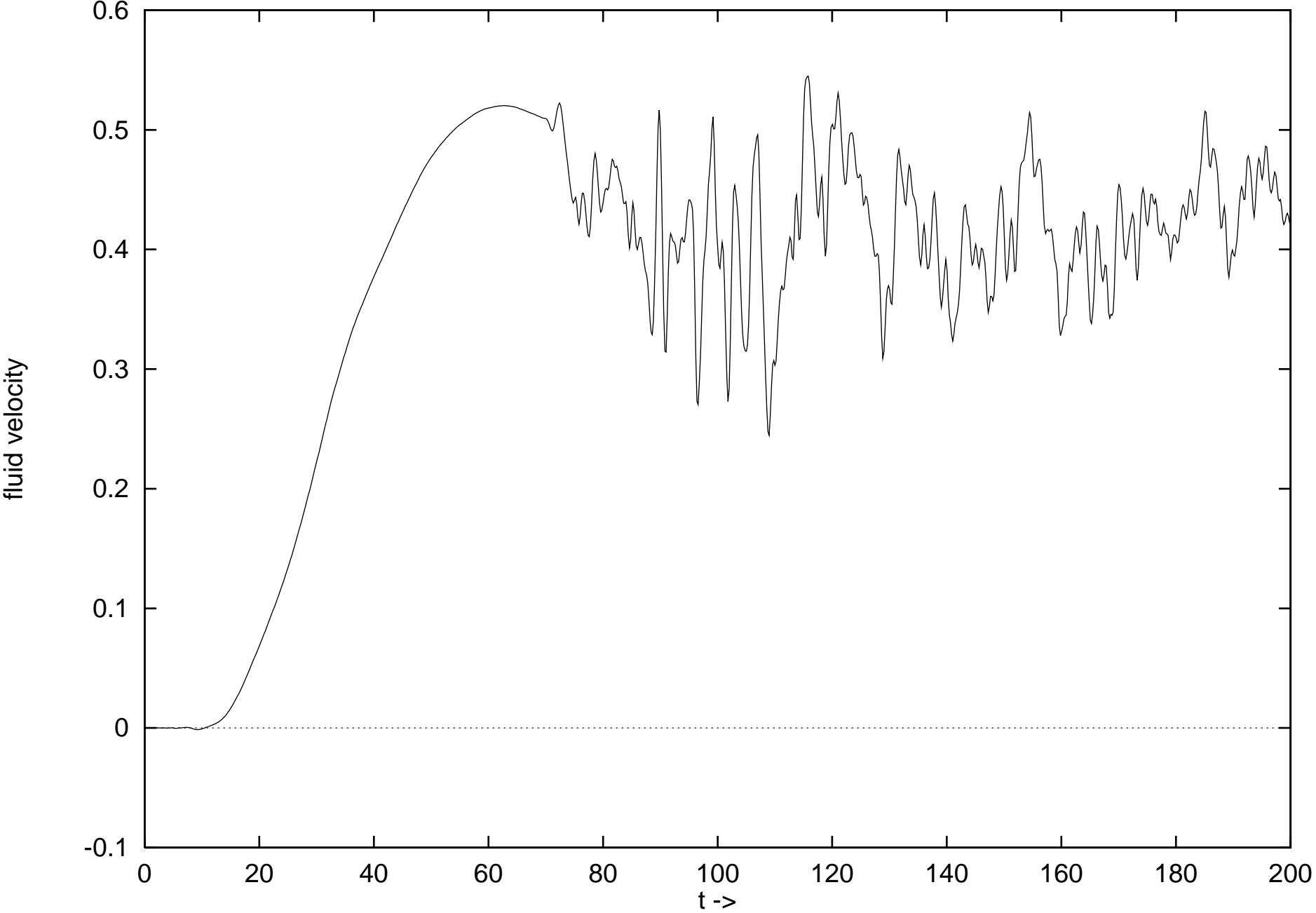


Fig. 4c

Plot of fluid velocity vs. time: round edges, wide orifice



Contour plot at t = 0.0

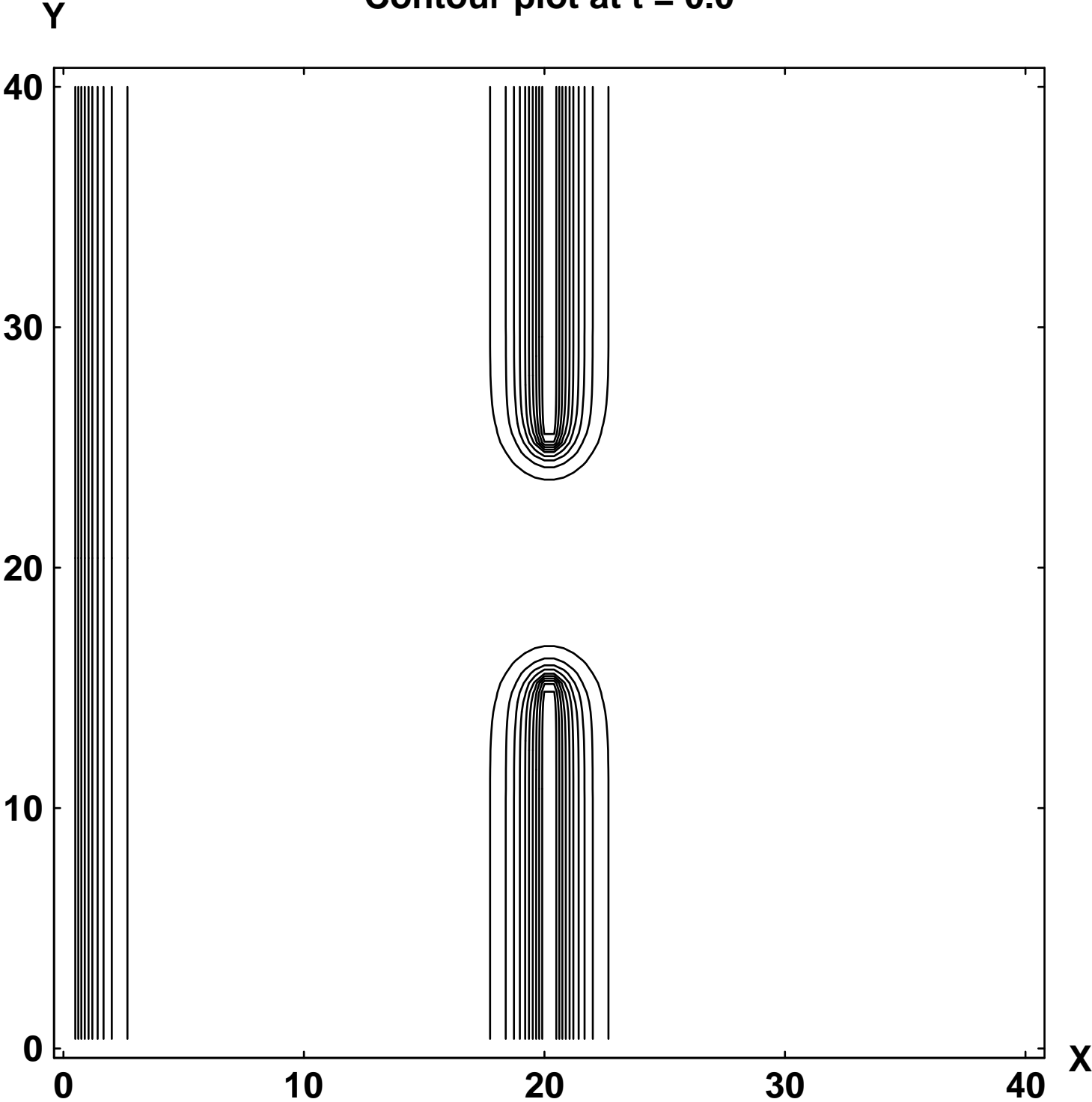


Fig. 1a

Contour plot at t = 76.0

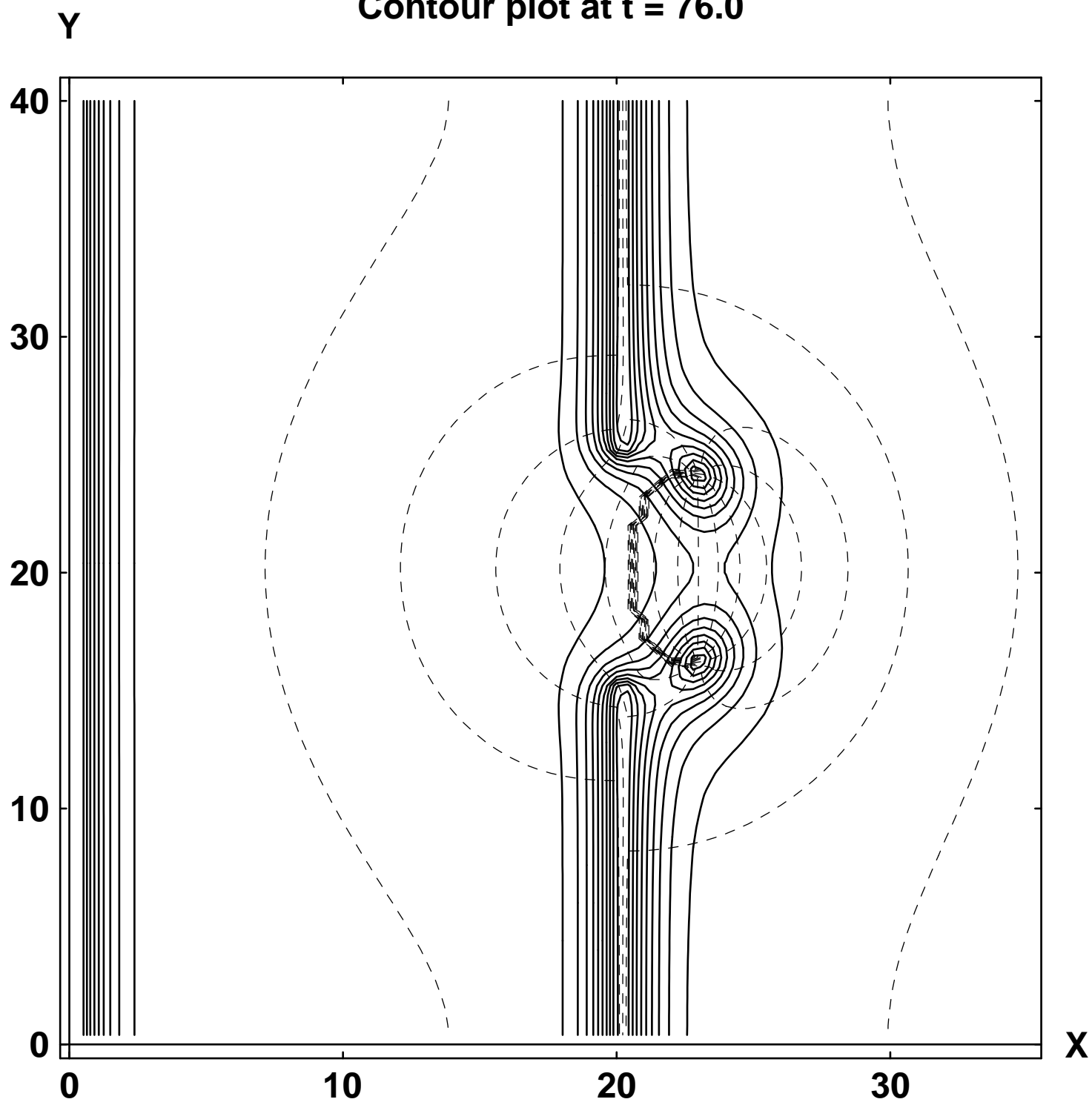


Fig. 4a

Plot of fluid velocity vs. time: sharp edges

